

Chapter 8

Full Duplex and Wireless-Powered Communications



Onel L. Alcaraz López and Hirley Alves

Abstract Wireless energy transfer (WET) is an attractive energy-efficient technology that has been identified as a potential enabler for the Internet of Things (IoT) era. Recently, there is an increasing interest in combining full duplex (FD) and WET to achieve greater system performance, and in this chapter we overview the main characteristics of the wireless-powered communication networks (WPCNs), the approaches for modeling the energy-harvesting (EH) conversion process, and the main FD architectures, namely (1) FD bidirectional communications, (2) FD relay communications, and (3) FD hybrid access point (AP), along with their particularities. We also discuss two example setups related with architectures (1) and (3), while demonstrating the suitable regions for FD operation in each case. For the former we demonstrate the gains in energy efficiency (EE) when the base station (BS) operates with FD for self-energy (SEg) recycling, while for the latter we show that the linear EH model is optimistic and that the FD design is not only simpler than half duplex's (HD) but it also can offer significant performance gains in terms of system reliability when the successive interference cancellation (SIC) hardware performs not too bad. Finally, some possible research directions for the design and deployment of FD wireless-powered systems are identified.

8.1 Introduction

With the advent of the Internet of Things (IoT) era, where communication systems should support a huge number of connected devices, there is an increasing interest in energy-efficient technologies. This is because (1) IoT devices are mostly low power and (2) powering and uninterrupted operation of such potential massive number of IoT nodes is a major challenge. Energy-harvesting (EH) techniques have recently drawn significant attention as a potential solution, and a variety of energy

O. L. A. López (✉) · H. Alves
University of Oulu, Centre for Wireless Communications, Oulu, Finland
e-mail: onel.alcarazlopez@oulu.fi; hirley.alves@oulu.fi

sources such as heat, light, and wind have been considered for EH in wireless networks [1]. These natural energy sources are usually location, weather, or climate dependent and may not always be available in enclosed/indoor environments or suitable for mobile devices. In that sense, wireless energy transfer (WET) [2], as a particular EH technique that allows the devices to harvest energy from radio-frequency (RF) signals, is very attractive because of the coverage advantages of RF signals, especially for IoT scenarios where replacing or recharging batteries requires high cost and/or can be inconvenient or hazardous (e.g., in toxic environments), or highly undesirable (e.g., for sensors embedded in building structures or inside the human body) [3].¹

Recently, there is an increasing interest in combining full duplex (FD) and WET to achieve greater system performance [4–31]. The reasoning behind is based on the fact that FD radios should not operate with very high transmit power due to the negative effect of the self-interference (SI), while path loss significantly limits the EH performance. Additionally, the idea of self-energy (SEg) recycling from the SI [14, 25, 26] has been shown to be beneficial by providing a secondary energy source, and consequently SI from the data transmission is no longer a nuisance to be strongly suppressed by an expensive hardware. Also, multiple-antenna setups are appropriate for both FD and WET operation since they help the receivers to accumulate more energy, while at the same time spatial SI cancellation techniques can be deployed [11, 16]. Therefore, incorporating FD operation in many WET systems will bring benefits in terms of increased spectral and energy efficiency (EE); of course, as long as the systems are properly designed.

8.1.1 *Wireless-Powered Networks: An Overview*

The idea of WET was first conceived and experimented by Nicola Tesla in 1899. However, the area did not pick up until the 1960s when microwave technologies rapidly advanced [2]. Nowadays, systems incorporating WET are becoming feasible due to the further advances in technology, the miniaturization of form factors, and availability of hardware with extremely low-power requirements, e.g., low-power sensors nodes. Actually, commercialization already began and one can find, for instance, PowerCast [32] and Cota system [33] products in the market.

Three main WET approaches have been identified in the literature:

1. Wireless EH, which refers to harvesting energy from the ambient RF signals, e.g., TV broadcasting, Wi-Fi, and GSM signals, and imposes some challenges due to the variable nature of the ambient RF signals, the path loss and shadowing vulnerability, and the choice of the rectifier since usually a range of frequencies must be scanned in order to harvest sufficient amounts of energy;

¹Note that we are referring to far-field RF energy transmission, which is different from (close contact) inductive RF energy transmission or nonradiative RF energy transmission.

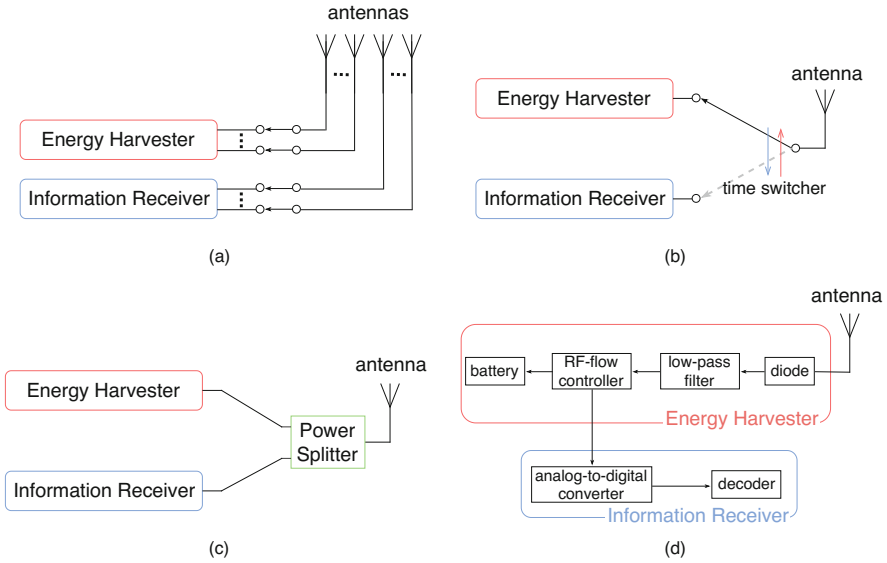


Fig. 8.1 Receiver architecture designs for SWIPT. (a) Separated receiver architecture; (b) time-switching architecture; (c) power splitting architecture; (d) integrated receiver architecture

2. Dedicated WET, which refers to harvesting energy using dedicated external sources such as a power beacon (PB). The gains depend on the placement of PBs, number of users to be served, the ability of the antenna array to focus the radiated power in the desired direction(s), and others; and
3. Simultaneous wireless information and power transfer (SWIPT), where both, information and RF energy, are conveyed from the source to the destination [34] using the same waveform, thus, saving spectrum.

With respect to SWIPT, four receiver architecture designs have been proposed and analyzed last years [35] (see Fig. 8.1):

- Separated receiver or antenna switching (AS) architecture is shown in Fig. 8.1a. The antenna array is divided into two sets with each connected to the EH circuitry or the information receiver. Consequently, this architecture allows to perform EH and information decoding independently and concurrently, and can be used to optimize the performance of separated receiver architecture as in [3].
- Co-located receiver architecture permits the EH and information receiver to share the same antenna(s). This architecture can be categorized into two models, e.g., time switching (TS) and power-splitting (PS) architectures, which are shown in Fig. 8.1b and c, respectively. When operating with TS, the network node switches and uses either the information receiver or the RF EH for the received RF signals at a time, while when operating with PS, the received RF signals are split into two streams for the information receiver and RF energy harvester with different power levels.

- Integrated receiver architecture [36] is shown in Fig. 8.1d. The implementation of RF-to-baseband conversion for information decoding is integrated with the energy harvester via the rectifier. The RF flow controller can also adopt a switcher or power splitter, like in the co-located receiver architecture, but the difference is that the switcher and power splitter are adopted in the integrated receiver architecture.

In general, the incident RF power at the EH receiver can be written as

$$P_{\text{RF}} = \left| \sum_{i=1}^T P_i [\mathbf{w}_i]_{1 \times N_i} [\mathbf{H}_i]_{N_i \times M} \mathbf{1}_{M \times 1} \right|^2, \quad (8.1)$$

or

$$P_{\text{RF}} = \sum_{i=1}^T \left| P_i [\mathbf{w}_i]_{1 \times N_i} [\mathbf{H}_i]_{N_i \times M} \mathbf{1}_{M \times 1} \right|^2, \quad (8.2)$$

where T is the number of energy transmitters, P_i , N_i , and \mathbf{w}_i are the overall transmit power, the number of transmit antennas, and the normalized complex precoding vector, e.g., $\|\mathbf{w}_i\|_2^2 = 1$, at the i -th energy transmitter, respectively, M is the number of EH antennas at the receiver, while \mathbf{H}_i is the complex channel matrix between the i -th energy transmitter and the EH receiver. Notice that (8.1) holds when the energy transmitters are fully synchronized and transmitting the same energy signals, while (8.2) holds when signals are fully independent. In both cases it is assumed a common EH circuitry for all receive antennas.

In case that the PS architecture is used, only a portion $\rho \in [0, 1]$ of this power goes to the RF-to-DC converter, while the remaining portion, $1 - \rho$, goes to the information decoding circuitry. Similarly, if TS scheme is utilized, the energy is harvested during a portion $\tau \in [0, 1]$ of the time, and the remaining portion, $1 - \tau$, is used for information decoding. Therefore, at the input of the RF-to-DC converter the RF power is $P_{\text{RF}}^* = \rho P_{\text{RF}}$ under PS, and $P_{\text{RF}}^* = P_{\text{RF}}$ during a portion τ of the time and $P_{\text{RF}}^* = 0$ the remaining portion under TS. Now, the harvested energy,² P_{DC} , can be written as a function of P_{RF}^* , as

$$P_{\text{DC}} = f(P_{\text{RF}}^*), \quad (8.3)$$

where $f : \mathcal{R} \rightarrow \mathcal{R}$ is a non-decreasing function of its argument. One important factor that limits the performance of a WET receiver is the RF-to-DC energy conversion efficiency. In fact, in most of the works f is assumed to be linear for

²We use the terms energy and power indistinctly, which can be interpreted as if harvesting time is normalized.

Table 8.1 Nonlinear EH models

$f(x)$	Reference	$f(x)$	Reference
$ce^{-ab}(e^{ab} - e^{-a(x-b)})(1 + e^{-a(x-b)})^{-1}$	[38]	$\frac{ax^3+bx^2+cx}{p_3x^3+p_2x^2+p_1x+p_0}$	[37]
$\frac{ax+b}{x+c} - \frac{b}{c}$	[16]	$ax^2 + bx + c$	[39]

analytical tractability, which implies that

$$f(x) = \eta x, \quad (8.4)$$

where η is a RF-to-DC energy conversion efficiency constant, thus, independent of the input power. However, many measurement data have revealed that the conversion efficiency actually depends on the input power [37] and consequently, the relationship between the input power and the output power is nonlinear. Table 8.1 summarizes the main nonlinear EH models in the literature where $a, b, c, p_3, p_2, p_1, p_0$ are constants determined by standard curve-fitting and are related to the detailed circuit specifications such as the resistance, capacitance, and diode turn-on voltage. The accuracy of the models depends on the fitting regions and on the specific characteristics of the EH circuits.

Finally, by just considering three factors such as (1) the sensitivity, which is the minimum RF input power required for energy harvesting, (2) the saturation level, which is the RF input power for which the diode starts working in the breakdown region and from that point onwards the output DC power keeps practically constant, and (3) a constant energy efficiency η between the sensitivity and saturation points; one can come up with a simple but accurate piece-wise model as illustrated in [40].

8.1.2 State of the Art on FD Wireless-Powered Networks

In the following we overview the recent results in FD wireless-powered communications separately according to three main topologies: FD bidirectional, FD relay, and FD hybrid access point (AP) communications, while other works are also discussed. Usually, the authors consider the harvest-use (HU) protocol, where the harvested energy cannot be stored and immediately must be consumed in order to maintain operability. A summary of the discussed results is shown in Table 8.2.

8.1.2.1 FD Bidirectional Communications

This kind of topology involves two-way information flow and one or two-way energy flow between the devices [4–7]. Specifically, the authors in [4] consider the PS architecture at EH receiver (one-way energy flow) and minimize the weighted sum transmit power by jointly designing the transmit beamforming vector of the

Table 8.2 Summary of the results on FD wireless-powered communications

Literature	Topology	WET approach and receiver architecture	Tuning parameter for optimization	Optimization goal
[4]	Bidirectional	SWIPT-PS	Transmit beamforming vector, ρ and the transmit power	Minimizing the weighted sum transmit power
[5]	Bidirectional	SWIPT-PS	Transmit power and ρ	Maximizing the sum-rate
[6]	Bidirectional	SWIPT-TS	Transmit beamforming vector, τ	Maximizing the UL throughput
[7]	Bidirectional	SWIPT-TS	τ , beamforming and transmit power	Maximizing the EE
[8]	Relay (AF/DF)	SWIPT-TS	τ	Maximizing the throughput
[9]	Relay (AF)	SWIPT-TS	τ	Minimizing outage probability
[10]	Relay (DF)	SWIPT-PS	ρ	Maximizing the end-to-end signal-to-interference-plus-noise ratio (SINR)
[11]	Relay (DF)	SWIPT-TS	Transmit and receive beamforming	Maximizing the end-to-end SINR
[12]	Relay (AF)	SWIPT-TS ($\tau = 1/2$)	Power allocation and transmit beamforming	Maximizing the throughput
[13]	Relay (DF)	SWIPT-TS	Receive and transmit beamformers, and τ	Maximizing the instantaneous throughput
[14]	Relay (AF)	SWIPT-TS ($\tau = 1/2$)	Beamforming	Maximizing signal-to-noise ratio (SNR)
[15]	Relay (AF/DF)	SWIPT-TS	Transmit beamforming (AF,DF) and τ (DF)	Maximizing the physical-layer security
[16]	Relay (AF)	SWIPT-TS/PS	Relay node	Minimizing outage probability
[17]	Hybrid AP	Dedicated WET	Antenna role	Ergodic capacity

(continued)

Table 8.2 (continued)

Literature	Topology	WET approach and receiver architecture	Tuning parameter for optimization	Optimization goal
[18]	Hybrid AP	Dedicated WET	DL and UL transmit powers and time slots duration	Maximizing the long-term weighted throughput
[19]	Hybrid AP	Dedicated WET	Time slots duration	Maximizing the throughput, and minimizing the total time
[20]	Hybrid AP	Dedicated WET	Transmit powers	Minimizing the aggregate power and maximizing the throughput
[21]	Hybrid AP	Dedicated WET	Subcarrier scheduling and transmit powers	Maximizing the sum-rate
[22]	Hybrid AP	Dedicated WET	Time slots duration and transmit power	Maximizing the throughput
[23]	Hybrid AP	Dedicated WET	Time slots duration	Maximizing the sum-throughput
[24]	Hybrid AP	Dedicated WET	DL beamforming and UL transmit power	Minimizing DL/UL transmit power and maximizing the total harvested energy
[25]	Hybrid AP	Dedicated WET	Duration of each phase, DL beamformers, and the UL transmit power	Maximizing the sum-rate, and EE
[26]	Hybrid FD/HD 4-node setup	SWIPT-PS	–	–
[27]	Relay (AF) with EH destination	SWIPT-PS	Beamforming	Minimizing MSE
[28]	Co-channel energy and information transfer	Dedicated WET	Energy and information beamformings	Maximizing the achievable data rate
[29]	FD friendly jammer	Dedicated WET	–	–

energy transmitter, the receive PS ratio, ρ , and the transmit power value of the EH device. The main limitation is that perfect successive interference cancellation (SIC) is assumed, which is not a practical assumption. Meanwhile, a point-to-point system where each two-antenna node houses identical transmitter–receiver pair is investigated in [5]. Each receiver intends to simultaneously transmit & decode information and harvests energy from the received signal. Therein, the authors propose transmit power and received PS ratio optimization algorithms that maximize the sum-rate subject to the transmit power and EH constraints. According to simulation results the residual SI may inhibit the system performance when it is not properly handled. On the other hand, some techniques for optimizing transmit beamforming in a FD multiple-input multiple-output (MIMO) setup, where the TS architecture is implemented at the EH receiver, are proposed in [6]. The problem is addressed when either complete instantaneous channel state information (CSI) or only its second-order statistics are available at the transmitter, while the authors demonstrate the advantages of the proposed methods over the sub-optimum and HD ones.

Finally, the potential of harvesting energy from the SI of a FD base station (BS) is further investigated in [7]. The BS is equipped with a SIC switch, which is turned off for a fraction of the transmission period for harvesting the energy from the SI that arises due to the downlink (DL) transmission. For the remaining transmission period, the switch is on such that the uplink (UL) transmission takes place simultaneously with the DL transmission. The authors explore the optimal time-splitting factor, τ , that maximizes the EE of the system along with the optimal beamforming and power allocation design for the DL and UL, respectively.

8.1.2.2 FD Relay Communications

A low-power FD relay node that assists the communications between the source and destination is powered by a WET process. The three-node FD relay wireless-powered communication network has been investigated in [8–15].

Both amplify and forward (AF) and decode and forward (DF) relaying protocols are studied in [8] using the TS architecture. An analytical characterization of the achievable throughput of three different communication modes, instantaneous transmission, delay-constrained transmission, and delay-tolerant transmission, is provided, while the optimal τ is investigated. It is shown that the FD relaying could substantially boost the system throughput compared to the conventional half duplex (HD) relaying architecture for the three transmission modes. An analysis of the outage probability in a TS AF FD setup is presented in [9] under imperfect channel state information (CSI). Numerical results provide some insights into the effect of various system parameters, such as τ , η , the noise power, and the channel estimation error on the performance of this network. Different from previous works, [10] explores both, the HU and harvest-use-store models, where the latter is implemented by switching between two batteries for charging and discharging with the aid of a PS architecture. A greedy switching policy is implemented with energy accumulation

across transmission blocks in the harvest-use-store model. Also, the optimal ρ is presented and the corresponding outage probability is derived by modeling the relay's energy levels as a Markov chain with a two-stage state transition.

The above works consider single-antenna source and destination nodes, while the relay is equipped with two antennas, one receive antenna for EH and information reception and one transmit antenna, which enables the FD operation. The case of multiple-input single-output (MISO) or multiple-input multiple-output (MIMO) relaying is considered in [11–15]. Three different interference mitigation schemes are studied in [11], namely (1) optimal, (2) zero-forcing (ZF), and (3) maximum ratio combining (MRC)/maximum ratio transmission (MRT), for a FD DF MIMO relaying system, and the authors attain outage probability expressions to investigate delay-constrained transmission throughput. In [12], the source is equipped with multiple antennas, while the FD MISO relay node operates with the AF protocol, and the authors find the optimal power allocation and beamforming design. The instantaneous throughput is maximized in [13], while results reveal how the relay beamforming, using MRC, ZF, and MRT, increases both the EH and SI suppression capabilities at the MIMO FD DF relay. The possibilities and limitations of SEg recycling for RF powered MIMO relay channels is studied in [14]. Therein, a geometric geodesic approach rendered a simple beamformer optimization for both DL only and joint up-down link protocols, providing efficient strategies for power allocation between data transmission and WET. The authors show that the hardware design for a high recycling ratio is the prerequisite for the proposed system to operate with EE. Different from previous literatures, in [15] an eavesdropper is threatening the information confidentiality in the last hop and the goal is to maximize the physical-layer security under harvested energy constraints. The authors show the trade-off between AF and DF protocols according to the occurrence probability of non-zero secrecy rate.

On a different note, [16] investigates a FD wireless-powered two-way communication networks, where two hybrid APs and multiple AF relays operate all in FD mode. Both, TS and PS, architectures are considered, the new time division duplexing static power splitting (TDD SPS) and the full duplex static power splitting (FDSPS) schemes as well as a simple relay selection strategy are proposed to improve the system performance.

8.1.2.3 FD Hybrid AP

Herein, data/energy from/to users in the UL/DL channel are transmitted and received simultaneously. The single user case is investigated in [17], where the serving user is also FD. The AP and user are both equipped with two antennas, one for WET from the AP to user and the other for UL WIT from the user to AP, where WET and WIT are performed simultaneously through the same frequency band. The role of each antenna (i.e., transmission or reception) is not predefined and the authors propose an antenna pair selection scheme to improve the system performance. The two-HD user scenario is studied in [18] where the focus is on

the long-term weighted throughput maximization problem. To that end, the analysis takes into account CSI variations over future slots and the evolution of the batteries when deciding the optimal resource allocation.

Different from above, the works in [19–25] analyze scenarios with an arbitrary number of serving users. In [19], the authors investigate the sum-throughput maximization problem and the total time minimization problem under perfect SIC for a setup where each user can continuously harvest wireless power from the AP until it transmits. Two distributed power control schemes for controlling the UL transmit power by the FD user equipments (UEs) and the DL energy-harvesting signal power by the FD AP are proposed in [20]. The objectives are minimizing the aggregate power subject to the quality of service requirement constraint and maximizing the aggregate throughput. Meanwhile, maximizing the sum-rate is the goal of the work in [21] where a joint subcarrier scheduling and power allocation algorithms for OFDM systems are investigated to that end. In [22], the authors design a protocol to support simultaneous WET in the DL and WIT in the UL by jointly optimizing the time allocations for WET and different users for UL WIT, and the transmit power allocations over time at the AP, such that the users' weighted sum-rate is maximized. With a similar setup, but now considering FD operation also at the UEs and with perfect SIC, the authors in [23] derive the optimal UL time allocation to users to maximize the network sum-throughput.

A new kind of systems comprising a FD AP, multiple single-antenna HD users and multiple energy harvesters equipped with multiple antennas, is considered in [24]. Therein, a multi-objective optimization taking into account heterogeneous quality of service requirements for UL and DL communication and WET is proposed, and the authors study the trade-off between UL and DL transmit power minimization and total harvested energy maximization. Finally, a system considering a FD multiple-antenna AP, multiple single-antenna DL users, and single-antenna UL users, where the latter need to harvest energy for transmitting information to the AP, is investigated in [25]. The communication is divided into two phases such that in the first one, the AP uses all available antennas for conveying information to DL users and wireless energy to UL users via information and energy beamforming, respectively, while in the second phase, UL users send their independent information to the AP using their harvested energy while the AP transmits the information to the DL users. The aim of the work is to maximize the sum rate and EE under UL user's achievable information throughput constraints by jointly optimizing beamforming and time allocation. In all the above works, the authors utilize the HD setup as benchmark while showing the benefits and limitations of the investigated FD operation.

8.1.2.4 Others

Herein we briefly discuss some works that do not fit, or at least not well, into the previous topologies. In [26], an energy-recycling single-antenna FD radio is designed by including a power divider and an energy harvester between the

circulator and the receiver chain. This brings advantages in terms of both spectral efficiency and energy consumption since it allows performing both, an arbitrary attenuation of the incoming signal and the recycling of a non-negligible portion of the energy leaked through the nonideal circulator. The authors analyze the performance gains of this architecture in a four-node scenario in which two nodes operate in FD and two nodes in HD, while they also provide valuable numerical results obtained under practical parameter assumptions. In [27], the authors consider a FD MIMO AF relay network but different from the works in Sect. 8.1.2.2 herein the destination node is the energy-limited node and performs SWIPT with the PS architecture. A joint optimization problem of source and relay beamformers under their transmit powers' constraints and the user's EH constraint is formulated and solved such that the mean-square-error (MSE) in the detection is minimized. In [28], the authors refer to a setup where the EH node harvests energy from a PB and at the same time and frequency it transmits its information to the destination, thus, a FD operation different than in all the previous works. The achievable data rate is maximized by jointly optimizing the energy beamforming at the PB and the information beamforming at the EH node subject to their individual transmit power constraints. Finally, a cooperative jamming protocol, termed as accumulate-and-jam (AnJ) is proposed in [29] to improve physical-layer security. This is done by deploying a FD EH friendly jammer to secure the direct communication between source and destination in the presence of a passive eavesdropper and under imperfect CSI.

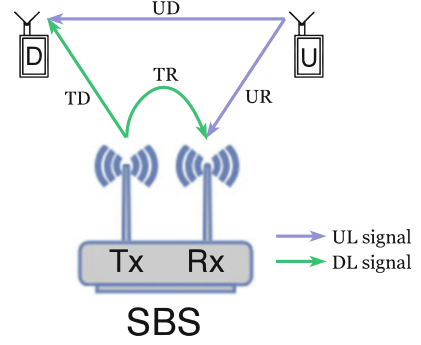
In the next two sections we present and analyze two example setups related with the FD bidirectional (Sect. 8.2) and FD hybrid AP (Sect. 8.3) architectures discussed previously. The suitable regions for FD operation are investigated in each case.

8.2 SEg Recycling for EE

Herein we consider a FD small cell BS (SBS) equipped with one transmit (T_x) and one receive (R_x) antenna, which serves one DL and one UL single-antenna UE, denoted as D and U , respectively. The SBS is powered by a regular grid source that can supply at most a power P_{\max} , and is also equipped with an RF EH device and a rechargeable battery for energy storage. The setup is represented in Fig. 8.2 where UD, TD, TR, UR denote the links $U \rightarrow D$, $T_x \rightarrow D$, $T_x \rightarrow R_x$, and $U \rightarrow R_x$, respectively. Notice that the system model corresponds to a FD bidirectional topology as described in Sect. 8.1.2.1. We assume quasi-static Rayleigh fading such that $h_{UD}, h_{UR}, h_{TD} \sim \text{Exp}(1)$ are the normalized power channel coefficients of the far-field links, which remain unchanged for a time block of duration T . Meanwhile, $g = h_{TR}$ is treated as a constant since this channel exhibits the near-field property different from the far-field fading [14, 41].

The transmission time is divided into phases of duration τT and $(1 - \tau)T$, and without loss of generality we set $T = 1$. In the first phase, the SBS transmits the information-bearing to D , while U is silent and the SIC switch in this phase is turned

Fig. 8.2 System model. FD SBS serving one DL and UL devices



off for SEg harvesting.³ Then, the received signal at D is given by

$$y_{d,1} = \sqrt{h_{TD}\varphi_{TD}(p_F + p_{EH})}s_d + w_d, \quad (8.5)$$

where s_d , $\mathbb{E}[|s_d|^2] = 1$, is the data signal from SBS and p_F and p_{EH} are the power that the SBS draws from the power grid and the power coming from the EH process. Thus, $p_F + p_{EH}$ constitutes the transmit power of the SBS. Additionally, φ_j denotes the path loss in the link $j \in \{UD, UR, TD\}$, and w_i is the complex additive white Gaussian noise (AWGN) at node $i \in \{D, U, SBS\}$ and we assume them with the same variance σ^2 . Since the EH process is also carried out in this phase when the SBS harvests the energy from the SI, the signal at R_x in the SBS is given by

$$y_{sbs,1} = \sqrt{g(p_F + p_{EH})}s_{sbs} + w_{sbs}, \quad (8.6)$$

where $\mathbb{E}[|s_{sbs}|^2] = 1$. Consequently, using the linear EH model in (8.4) the SEg harvested at the SBS in the first phase is given by

$$E = \eta\tau\mathbb{E}[|y_{sbs,1}|^2] = \eta\tau g(p_F + p_{EH}), \quad (8.7)$$

where the noise term is ignored in the last step as its contribution is negligible. Since the energy E in (8.7) is going to be used during the entire block (of unit duration) for transmission by assisting the power-grid consumption, we have that $E = p_{EH}$ and there is an energy loop described by

$$p_{EH} = \eta\tau g(p_F + p_{EH}) = \frac{\eta\tau g p_F}{1 - \eta\tau g}, \quad (8.8)$$

where the last step comes from isolating p_{EH} in the first line. Notice that since $\eta, \tau, g < 1$ we have that $1 - \eta\tau g > 0$.

³ U keeps silent in this phase since channel UR is not sufficiently strong for WET, thus, the SBS only relies on the SEg for EH purpose.

In the second phase, the SBS turns the SIC switch on, which causes an attenuation $\zeta \ll 1$ of the SI signal, thus, the signal received at R_x in the SBS is given as

$$y_{\text{sbs},2} = \sqrt{h_{\text{UR}}\varphi_{\text{UR}}p_{\text{U}}s_u} + \sqrt{\zeta g(p_{\text{F}} + p_{\text{EH}})s_{\text{sbs}}} + w_{\text{sbs}}, \quad (8.9)$$

with $\mathbb{E}[|s_u|^2] = 1$, and the instantaneous SINR is

$$\gamma_{\text{sbs}} = \frac{h_{\text{UR}}\varphi_{\text{UR}}p_{\text{U}}}{\zeta g(p_{\text{F}} + p_{\text{EH}}) + \sigma^2} = \frac{h_{\text{UR}}\varphi_{\text{UR}}p_{\text{U}}}{\frac{\zeta g p_{\text{F}}}{1-\eta\tau g} + \sigma^2}, \quad (8.10)$$

where the last step comes from using (8.8). Meanwhile, the signal received at D in this phase is given by

$$y_{\text{d},2} = \sqrt{h_{\text{TD}}\varphi_{\text{TD}}(p_{\text{F}} + p_{\text{EH}})s_d} + \sqrt{h_{\text{UD}}\varphi_{\text{UD}}p_{\text{U}}s_u} + w_d. \quad (8.11)$$

Notice that different from (8.5), in (8.11) it is reflected the impact of the interference coming from U . The impact of this interference is for $1 - \tau$ portion of the time, thus, we can write the instantaneous SINR at D for the whole block duration as

$$\begin{aligned} \gamma_{\text{d}} &= \frac{h_{\text{TD}}\varphi_{\text{TD}}(p_{\text{F}} + p_{\text{EH}})}{(1 - \tau)h_{\text{UD}}\varphi_{\text{UD}}p_{\text{U}} + \sigma^2} \\ &= \frac{h_{\text{TD}}\varphi_{\text{TD}}p_{\text{F}}}{(1 - \eta\tau g)((1 - \tau)h_{\text{UD}}\varphi_{\text{UD}}p_{\text{U}} + \sigma^2)}, \end{aligned} \quad (8.12)$$

where the last step comes from using (8.8).

8.2.1 Problem Formulation

We assume delay-limited transmission for both DL and UL links such that each destination node has to decode the received signal block by block, and the transmit rates (r_{d} and r_{sbs} , respectively) are assumed fixed for many consecutive blocks and established according to transmitter and/or receiver requirements. Therefore, the outage event in the link TD, UR is defined as $\mathbb{O}_{\text{d}} \triangleq \{\log_2(1 + \gamma_{\text{d}}) < r_{\text{d}}\}$ and $\mathbb{O}_{\text{sbs}} \triangleq \{(1 - \tau) \log_2(1 + \gamma_{\text{sbs}}) < r_{\text{sbs}}\}$, respectively. Meanwhile, the power consumed from the grid at the SBS and from the battery or grid source at U and D is given by

$$P_{\text{con}} = \frac{p_{\text{F}} + p_{\text{U}}(1 - \tau)}{\epsilon} + P_{\text{cir},1} + P_{\text{cir},2}, \quad (8.13)$$

where ϵ is the amplifier efficiency at the SBS and U ; and $P_{\text{cir},1}$, $P_{\text{cir},2}$ is the circuit consumption at the SBS, and the total circuit consumption at D and U , respectively.

In compliance with 5G networks, we maximize the system's EE by jointly designing p_F and τ . Notice that τ^* (optimum τ) might be equal to zero, and in such case SEg is not beneficial for the system performance. We measure the EE as the ratio between the throughput and the aggregated energies drawn from any source but from the SEg recycling process. Therefore,

$$\text{EE} = \frac{r_d(1 - \mathbb{P}[\mathbb{O}_d]) + r_{\text{sbs}}(1 - \mathbb{P}[\mathbb{O}_{\text{sbs}}])}{P_{\text{con}}}, \quad (8.14)$$

and the optimization problem is stated as follows:

$$\mathbf{P1} : \quad \arg \max_{p_F, \tau} \quad \text{EE} \quad (8.15a)$$

$$\text{s.t.} \quad 0 \leq \tau \leq 1, \quad (8.15b)$$

$$\frac{p_F}{\epsilon} + P_{\text{cir},1} \leq P_{\text{max}}. \quad (8.15c)$$

In the next subsection we characterize the outage performance in TD, UR links as it is required for evaluating (8.14).

8.2.2 Outage Analysis

We proceed as follows:

$$\begin{aligned} \mathbb{P}[\mathbb{O}_d] &= \mathbb{P}[\log_2(1 + \gamma_d) < r_d] \stackrel{(a)}{=} \mathbb{P}[\gamma_d < 2^{r_d} - 1] \\ &\stackrel{(b)}{=} \mathbb{P}\left[\frac{h_{\text{TD}}\varphi_{\text{TD}}p_F}{(1 - \eta\tau g)((1 - \tau)h_{\text{UD}}\varphi_{\text{UD}}p_U + \sigma^2)} < 2^{r_d} - 1\right] \\ &\stackrel{(c)}{=} \mathbb{P}\left[h_{\text{TD}} < \frac{(2^{r_d} - 1)(1 - \eta\tau g)((1 - \tau)h_{\text{UD}}\varphi_{\text{UD}}p_U + \sigma^2)}{\varphi_{\text{TD}}p_F}\right] \\ &\stackrel{(d)}{=} 1 - \mathbb{E}\left[e^{-(b_1 + b_2 h_{\text{UD}})}\right] \stackrel{(e)}{=} 1 - \frac{e^{-b_1}}{1 + b_2}, \end{aligned} \quad (8.16)$$

where (a) comes from isolating γ_d , (b) comes from using (8.12), (c) is attained by isolating h_{TD} , while (d) follows by using its cumulative distribution function (CDF) along with

$$b_1 = (2^{r_d} - 1)(1 - \eta\tau g) \frac{\sigma^2}{\varphi_{\text{TD}}p_F}, \quad (8.17)$$

$$b_2 = (2^{r_d} - 1)(1 - \eta\tau g)(1 - \tau) \frac{\varphi_{\text{UD}}p_U}{\varphi_{\text{TD}}p_F}, \quad (8.18)$$

and finally, (e) is the result of computing the expectation with respect to the exponential random variable (RV) h_{UD} .

In the case of $\mathbb{P}[\mathbb{O}_{\text{sbs}}]$ we proceed as follows:

$$\begin{aligned}
 \mathbb{P}[\mathbb{O}_{\text{sbs}}] &= \mathbb{P}[(1 - \tau) \log_2(1 + \gamma_{\text{sbs}}) < r_{\text{sbs}}] \stackrel{(a)}{=} \mathbb{P}\left[\gamma_{\text{sbs}} < 2^{\frac{r_{\text{sbs}}}{1-\tau}} - 1\right] \\
 &\stackrel{(b)}{=} \mathbb{P}\left[\frac{h_{\text{UR}}\varphi_{\text{UR}}P_{\text{U}}}{\frac{\xi g_{\text{PF}}}{1-\eta\tau g} + \sigma^2} < 2^{\frac{r_{\text{sbs}}}{1-\tau}} - 1\right] \stackrel{(c)}{=} \mathbb{P}\left[h_{\text{UR}} < \frac{\left(2^{\frac{r_{\text{sbs}}}{1-\tau}} - 1\right)\left(\frac{\xi g_{\text{PF}}}{1-\eta\tau g} + \sigma^2\right)}{\varphi_{\text{UR}}P_{\text{U}}}\right] \\
 &\stackrel{(d)}{=} 1 - e^{-\frac{\left(2^{\frac{r_{\text{sbs}}}{1-\tau}} - 1\right)\left(\frac{\xi g_{\text{PF}}}{1-\eta\tau g} + \sigma^2\right)}{\varphi_{\text{UR}}P_{\text{U}}}}, \tag{8.19}
 \end{aligned}$$

where (a) comes from isolating γ_{sbs} , (b) comes from using (8.10) along with (8.8), (c) is attained by isolating h_{UR} , while (d) follows by using its CDF.

8.2.3 Numerical Solution

Based on the results in the previous subsection, **P1** in (8.15) can be stated as

$$\mathbf{P2} : \quad \arg \max_{p_{\text{F}}, \tau} \quad \frac{r_{\text{d}} \frac{e^{-b_1}}{1+b_2} + r_{\text{sbs}} e^{-\frac{\left(2^{\frac{r_{\text{sbs}}}{1-\tau}} - 1\right)\left(\frac{\xi g_{\text{PF}}}{1-\eta\tau g} + \sigma^2\right)}{\varphi_{\text{UR}}P_{\text{U}}}}}{\frac{p_{\text{F}} + p_{\text{U}}(1-\tau)}{\epsilon} + P_{\text{cir},1} + P_{\text{cir},2}} \tag{8.20a}$$

$$\text{s.t.} \quad 0 \leq \tau \leq 1, \tag{8.20b}$$

$$p_{\text{F}} \leq \epsilon(P_{\text{max}} - P_{\text{cir},1}). \tag{8.20c}$$

Notice that **P2** would be cumbersome to solve in closed-form because of the tangled dependence of the objective function on p_{F} and τ . Since convexity analysis seems also a cumbersome task (in fact, numerical results show that the objective function is not concave), herein we resort to numerical methods to solve **P2** while drawing some insights from the numerical results. We assume $\varphi_{\text{TD}} = \varphi_{\text{UR}} = \varphi_{\text{UD}} = \varphi$ and unless stated otherwise the parameter values are those presented in Table 8.3.

Figure 8.3 shows a contour plot of EE vs τ , p_{F} . As clearly shown in the figure, the objective function in **P2** is not concave because of the presence of two local peaks: one maximum and one minimum, and any algorithm for solving the optimization problem has to deal with that issue. Notice that $p_{\text{F}}^* = 25$ dBm and most interesting $\tau^* \approx 0.42$ which is much larger than 0; thus, SEg harvesting results are advantageous for improving the EE of the system. The success probabilities at that operation point are 0.63 and 0.99 for TD and UR links, respectively.

In Fig. 8.4, we show the optimization results as functions of r_{sbs} for different transmit power levels at U and transmit rates in the DL. As shown in Fig. 8.4a,

Table 8.3 System parameters for setup in Fig. 8.2

Parameter	Value	
p_U	25 dBm	
P_{\max}	40 dBm	
η	0.5	[4, 7, 16]
ε	0.69	[7]
r_d, r_{sbs}	1, 5 bps/Hz	
φ	10^{-5}	
σ^2	-70 dBm	[4]
g, ζ	-15, -110 dB	[7, 12]
$P_{\text{cir},1}, P_{\text{cir},2}$	30, 40 dBm	[7]

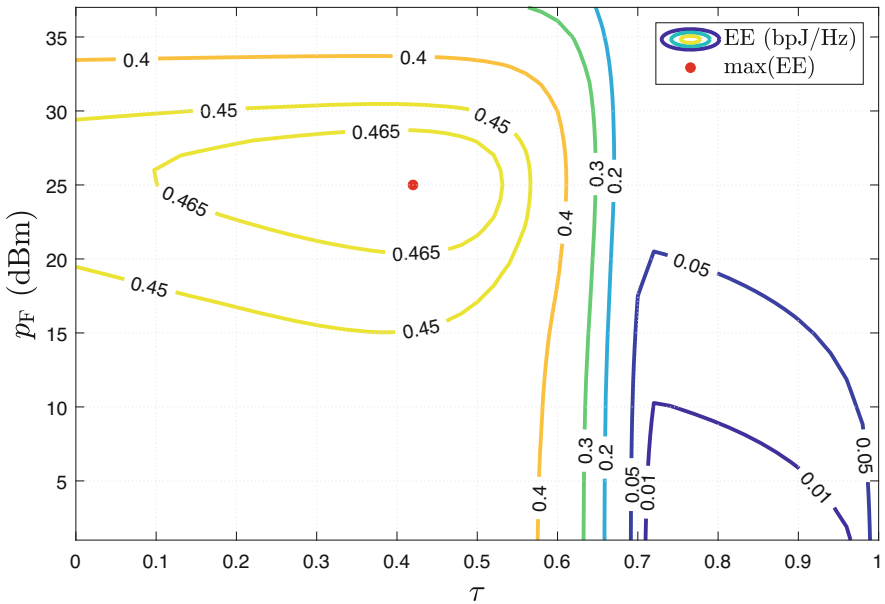


Fig. 8.3 EE as a function of p_F and τ

only for relatively large data rates in the UL, the SEg harvesting is not beneficial since $\tau \rightarrow 0$. A smaller p_U and/or DL transmit rate makes SEg less beneficial. In the first case because the success probability in the UL becomes more dependent on the transmission time since the U 's transmit power decreases; while in the second case, when the DL transmit rate is small, less power resources at the SBS are necessary, which is also shown in Fig. 8.4b, thus, the need of SEg decreases. Interesting, Fig. 8.4b shows that as p_U increases, p_F^* increases as well in almost all the region. The region for which this holds is particularly dependent on to the specific values of r_{sbs} and r_d , and notice that for $r_{\text{sbs}} \geq 7$ bps/Hz and $r_d = 1$ bps/Hz, such relation no longer holds. The abrupt changes in the red lines in that region reflect the interplay of both, UL and DL throughputs, where the r_{sbs} values at

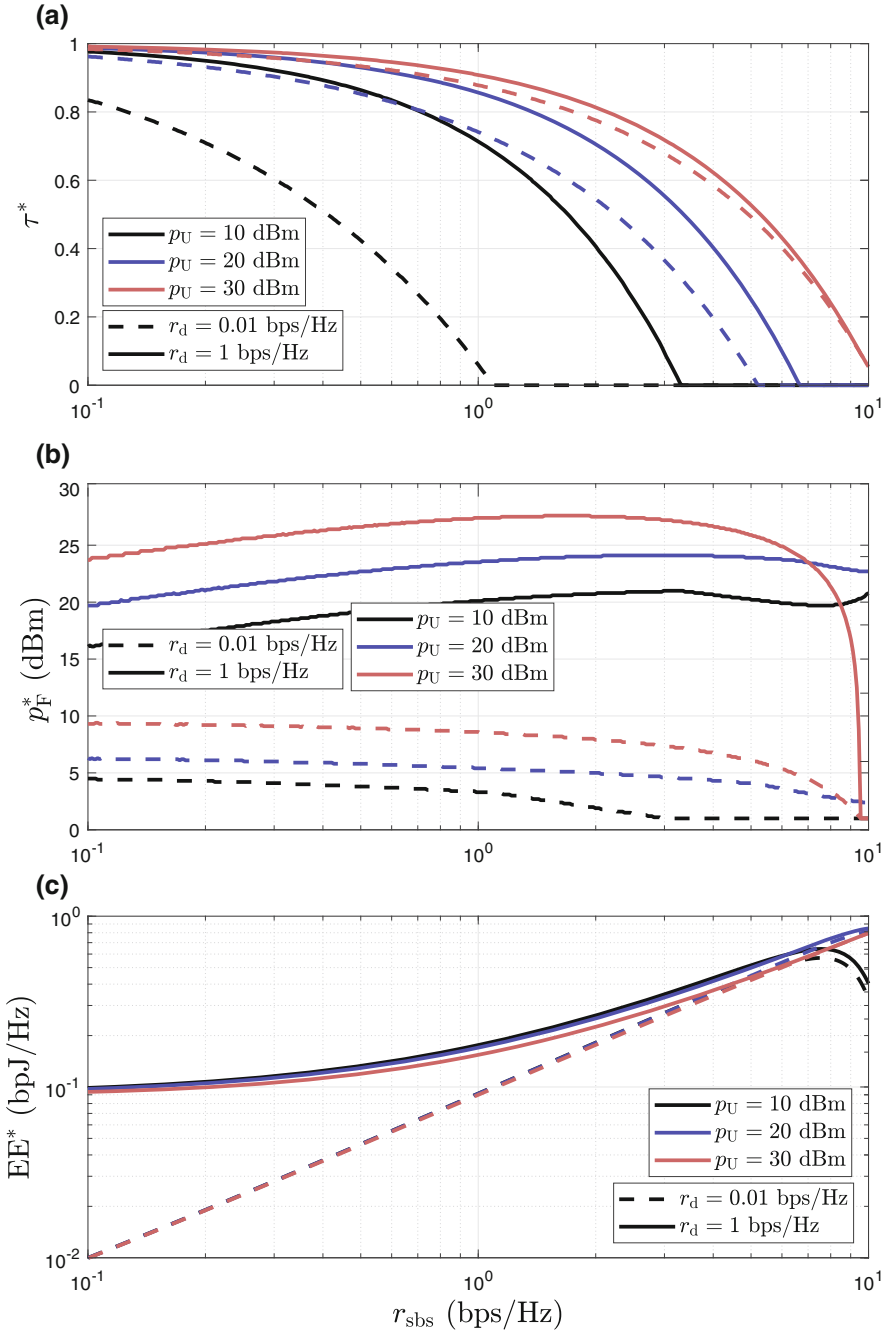


Fig. 8.4 (a) τ^* (top), (b) p_F^* (middle), and (c) EE^* (bottom), as a function of r_{sbs} for $p_U \in \{10, 20, 30\}$ dBm and $r_d \in \{0.01, 1\}$ bps/Hz

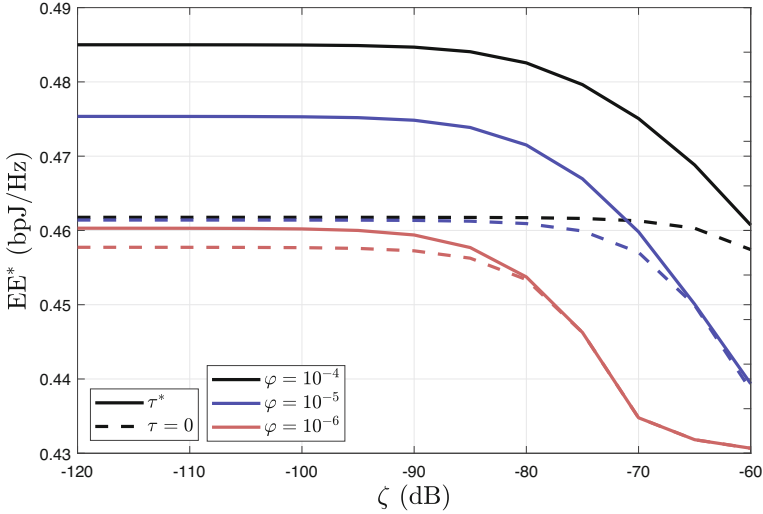


Fig. 8.5 EE^* as a function of ζ for $\varphi \in \{10^{-4}, 10^{-5}, 10^{-6}\}$ with/without SEg recycling

the changing points determine when UL or DL throughputs become more relevant between each other. The EE values attained with the optimum allocation are shown in Fig. 8.4c and notice that the system is more energy efficient when p_U is around 20 dBm. Also, from $r_{\text{sbs}} = 7.5$ bps/Hz onwards the EE is no longer increasing on r_{sbs} for $p_U = 10$ dBm because the UL success probability affects heavily the UL throughput.

Finally, in Fig. 8.5 we show the optimum EE as a function of the SIC performance parameter for the case with and without SEg harvesting and for different path-loss attenuations. As expected, as the path loss becomes more critical, the EE decreases, but also the SEg harvesting becomes less beneficial. Additionally, the better the SIC performance (smaller ζ) is, more gain from SEg harvesting can be obtained. This is because, SIC performance affects directly the UL success probabilities, and when SIC is relatively high, the impact of the UL transmission time becomes more important and τ^* decreases.

8.3 FD for Sporadic IoT Transmissions

In this subsection we consider a FD SBS serving k single-antennas IoT devices, referred as UEs. The SBS is assumed to be equipped with two antennas. One is for the DL WET, while the other one is used to receive the UL information transmission from the users (WIT). Thus, the normalized channel power gains for the DL channel, h_i , and UL channel, g_i , are different, and the topology matches the FD Hybrid AP model described in Sect. 8.1.2.3. The system setup is illustrated in Fig. 8.6, and we

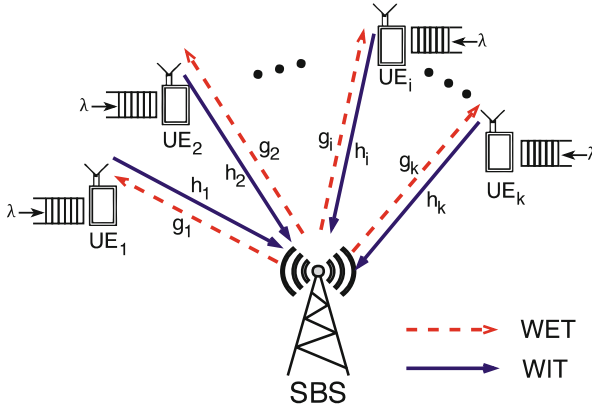


Fig. 8.6 System model. FD SBS serving k UEs with Poisson traffic

<u>FD Operation</u>	<u>HD Operation</u>
<ol style="list-style-type: none"> 1. The entire time block is divided in δ slots. Thus, each time slot has duration of $1/\delta$. 2. UEs are continuously harvesting energy until a message arrives to its output buffer. 3. After a data message arrives, the UE keeps harvesting energy until the current time slot ends, and then it transmits the message in the following time slot using all the harvested energy. 	<ol style="list-style-type: none"> 1. The entire time block is divided in two parts. The first part, of duration $\tau < 1$, is used only for WET from the SBS to the UEs, while the second part, of duration $1 - \tau$, is divided in δ time slots. Thus, each time slot has duration of $(1 - \tau)/\delta$. 2. When a message arrives to the UE's output buffer, it selects randomly one transmit time slot from those that are still to come and transmits over it.

Fig. 8.7 Operation scheme

assume quasi-static fading, e.g., such that channel remains unchanged during the duration T of a block, and varies independently from one block to another one. We assume that all the links are subject to the same path-loss attenuation φ , and without loss of generality we set $T = 1$.

We assume sporadic and short transmissions, which are typical characteristics of future IoT networks [42]. Hence, we model the arrivals of data messages of fixed length d (in bits/Hz) to the first-in first-out (FIFO) queue buffer before transmission, as a Poisson RV with rate $\lambda \ll 1$ (in mssg/block—messages per block). Thus, the inter-arrivals time, β (in blocks), is exponentially distributed with mean $1/\lambda$.

8.3.1 Slotted Operation

The operation procedure is illustrated in Fig. 8.7 for the FD scheme and the HD operation counterpart which is used as benchmark. Notice that, for the HD scheme

there is only one antenna available at the SBS. Additionally, since $\lambda \ll 1$, the chances of two (or more) consecutive messages arriving to be transmitted in the same time slot is small, and because it is a rare event and for simplicity, we assume that the second message cannot be delivered.

8.3.2 FD Performance

By denoting p_T as the SBS transmit power, the energy available for harvesting at the i -th UE in the j -th time slot, is approximately given by

$$E_i^{(j)} = \frac{p_T \varphi g_i^{(j)}}{\delta}, \quad (8.21)$$

where the contribution of the noise energy and UL signals from other UEs in the same slot was ignored. Notice that the transmit power of the low-power UEs that are concurrently transmitting in the j -th slot is much smaller than the powering signal coming from the SBS, therefore its contribution would be negligible unless they are very close from the harvesting device. Herein, we assume its energy contribution is negligible. On the other hand, because of the quasi-static property we have that $g_i^{(n\delta+1)} = g_i^{(n\delta+2)} = \dots = g_i^{((n+1)\delta)}$, where $i = 1, \dots, k$ and $n = 0, 1, \dots$, which also holds for the UL channels, h_i .

We consider the two EH models discussed at the end of Sect. 8.1.1. Therefore, after the WET phase, which lasts for $\lceil \delta\beta_i \rceil$ consecutive time slots for UE $_i$, the transmit power is a RV that can be expressed as

$$p_i = \sum_{j=1}^{\lceil \delta\beta_i \rceil} f(\delta E_i^{(j)}) = \sum_{j=1}^{\lceil \delta\beta_i \rceil} f(p_T \varphi g_i^{(j)}), \quad (8.22)$$

which for the case of the linear model in (8.4) reduces to $p_i = \eta p_T \varphi \sum_{j=1}^{\lceil \delta\beta_i \rceil} g_i^{(j)}$.

At the SBS side, the received signal in a given time slot j is given by

$$y_j = \sum_{i=1}^k \sqrt{h_i^{(j)} \varphi p_i \chi_i^{(j)}} s_i + \sqrt{\psi p_T} s_{ue} + \omega_{sbs}, \quad (8.23)$$

where s_i , $\mathbb{E}[|s_i|^2] = 1$, is the data signal from UE $_i$ and $\chi_i^{(j)}$ denotes the activity of that UE in the time slot j , this is, $\chi_i^{(j)} = 1$ or $\chi_i^{(j)} = 0$ if UE $_i$ is active or inactive, respectively. More formally,

$$\chi_i^{(j)} = \mathbb{I}(\text{mod}(\lceil \delta\beta_i \rceil, \delta) + 1 = j), \quad (8.24)$$

where $\text{mod}(\cdot, \cdot)$ is the modulo operation and $\mathbb{I}(\cdot)$ is the indicator function, which is equal to the unity if the argument is true; otherwise, its output is zero. Finally, ψ accounts for the combined effect of the SI channel attenuation and the SIC performance, which similarly to the scenario in the previous subsection is assumed as a constant; and ω_{sbs} is the complex AWGN at the SBS with variance σ^2 . In case of several UEs transmitting in the same time slot, successive interference cancellation (also referred as SIC) is carried out when decoding. Therefore, herein we are interested in SINR after SIC in order to evaluate the system performance. For ease of exposition let us sort the UEs in descending order according to the value of $h_i^{(j)} \varphi p_i \chi_i^{(j)}$, thus, UE_i is the i -th UE in the list, and assuming it is active and the first $l = 1, \dots, i - 1$ UEs were correctly decoded, its SINR is given by

$$\text{SINR}_i^{(j)} = \frac{h_i^{(j)} \varphi p_i}{\varphi \sum_{l=i+1}^k h_l^{(j)} p_l \chi_l^{(j)} + \psi p_T + \sigma^2}. \quad (8.25)$$

Notice that $\sum_{l=i+1}^k h_l^{(j)} p_l \chi_l^{(j)} = 0$ when $i = k$.

There is success in decoding the information from the i -th UE in the j -th time slot when $\text{SINR}_i^{(j)} > 2^{d\delta} - 1$ and the data from the l -th UEs ($l = 1, \dots, i - 1$) were also decoded correctly. Thus, the overall system reliability is defined as

$$P_{\text{succ}}^{\text{fd}} = \mathbb{E} \left[\frac{\sum_{i=1}^k \mathbb{I}(\text{SINR}_1^{(j)} > 2^{d\delta} - 1) \times \dots \times \mathbb{I}(\text{SINR}_i^{(j)} > 2^{d\delta} - 1)}{\sum_{i=1}^k \chi_i^{(j)}} \right], \quad (8.26)$$

where the expectation is taken with respect to the fading realizations and user activity, which depends on the traffic characteristics. Notice that outage events for the concurrent transmitting UEs are correlated, thus, numerator in (8.26) cannot be further efficiently simplified.

8.3.3 HD Performance

In the HD scenario, the UEs are harvesting energy during a portion τ of the block time. Therefore, the energy harvested in the j -th block by UE_i is given by

$$E_i^{(j)} = \tau p_T \varphi g_i^{(j)}, \quad (8.27)$$

whereas in the previous case, the noise energy is ignored. Notice that for FD j identifies a time slot, while here it identifies a whole block. Now, after the WET procedure, which lasts for $\lceil \beta_i \rceil$ consecutive blocks but without including the last

$(1 - \tau)$ portion of each block, the transmit power of UE $_i$ in its transmit slot is

$$p_i = \frac{\tau \delta}{1 - \tau} \sum_{j=1}^{\lceil \beta_i \rceil} f\left(\frac{E_i^{(j)}}{\tau}\right), \quad (8.28)$$

which for the case of the linear model in (8.4) reduces to $p_i = \frac{\tau \delta \eta p_T \varphi}{1 - \tau} \sum_{j=1}^{\lceil \beta_i \rceil} g_i^{(j)}$.

At the SBS side, the received signal in a given time slot j is given by

$$y_j = \sum_{i=1}^k \sqrt{h_i^{(j)}} \varphi p_i \chi_i^{(j)} s_i + \omega_{\text{sbs}}, \quad (8.29)$$

and again $\chi_i^{(j)}$ denotes the activity of UE $_i$ in the time slot j , which according to the procedure described in Fig. 8.7 for HD is now given by

$$\chi_i^{(j)} = \begin{cases} \mathbb{I}(v = j), & \text{if } \beta_i - \lfloor \beta_i \rfloor \leq \tau \text{ or } \beta_i - \lfloor \beta_i \rfloor > \tau + \frac{(\delta-1)(1-\tau)}{\delta} \\ \mathbb{I}(v = j), & \text{otherwise} \end{cases}, \quad (8.30)$$

where v , v are discrete RVs with PMFs given by $\mathbb{P}(v = j) = 1/\delta$ for $j = 1, \dots, \delta$ and $\mathbb{P}(v = j) = 1/(\delta - \rho)$ for $j = \rho + 1, \rho + 2, \dots, \delta$, respectively. In the latter expression ρ is the smallest non-negative integer that satisfies $\beta_i - \lfloor \beta_i \rfloor - \tau < \rho(1 - \tau)/\delta$ for $\rho < \delta$, thus, $\rho = \lceil \delta(\beta_i - \lfloor \beta_i \rfloor - \tau)/(1 - \tau) \rceil$. In a simplified form we can state $\mathbb{P}(v = j) = 1/(\delta - \text{mod}(\lceil \delta(\beta_i - \lfloor \beta_i \rfloor - \tau)/(1 - \tau) \rceil, \delta))$.

Once again, as in the FD case, in case of several UEs transmitting in the same time slot, SIC is carried out when decoding. By sorting the UEs in descending order according to the value of $h_i^{(j)} \varphi p_i \chi_i^{(j)}$, and assuming UE $_i$ is active and the first $l = 1, \dots, i - 1$ UEs were correctly decoded, its SINR is given by

$$\text{SINR}_i^{(j)} = \frac{h_i^{(j)} \varphi p_i}{\varphi \sum_{l=i+1}^k h_l^{(j)} p_l \chi_l^{(j)} + \sigma^2}. \quad (8.31)$$

and again $\sum_{l=i+1}^k h_l^{(j)} p_l \chi_l^{(j)} = 0$ when $i = k$.

There is success in decoding the information from the i -th UE in the j -th time slot when $\text{SINR}_i^{(j)} > 2^{\frac{d\delta}{1-\tau}} - 1$ and the data from the l -th UEs ($l = 1, \dots, i - 1$) were also decoded correctly. Thus, the overall system reliability is defined as

$$P_{\text{succ}}^{\text{hd}} = \mathbb{E} \left[\frac{\sum_{i=1}^k \mathbb{I}\left(\text{SINR}_1^{(j)} > 2^{\frac{d\delta}{1-\tau}} - 1\right) \times \dots \times \mathbb{I}\left(\text{SINR}_i^{(j)} > 2^{\frac{d\delta}{1-\tau}} - 1\right)}{\sum_{i=1}^k \chi_i^{(j)}} \right], \quad (8.32)$$

where the expectation is taken with respect to the fading realizations and user activity, which depends on the traffic characteristics. Notice that outage events for the concurrent transmitting UEs are correlated, thus, numerator in (8.26) cannot be further efficiently simplified.

8.3.4 Performance Analysis

In this subsection we use Monte Carlo simulations to analyze the system performance under different settings. We obtain the results for the ideal linear EH model presented in (8.4) and a suitable nonlinear EH model.

To that end we assume that the UEs are equipped with the EH hardware proposed in [43]. The input–output power relation for the measurement data offered in [43] is shown in Fig. 8.8, and we compare the different EH models discussed in Sect. 8.1.1 for that specific hardware. Notice that the linear model is suitable for the range of small input power but it fails mimicking the saturation region. As shown in the figure, the nonlinear model in [38] performs the best, and the saturation is ensured for values greater than 1000 μW since it is based on a logistic function, different from the other nonlinear models. Therefore, we adopt the nonlinear model in [38] as well as the linear alternative with $\eta = 0.07$. Finally, channels are assumed i.i.d with Nakagami- m fading, such that $h_i, g_i \sim \Gamma(m, 1/m)$, and unless stated otherwise the parameter values are those presented in Table 8.4.

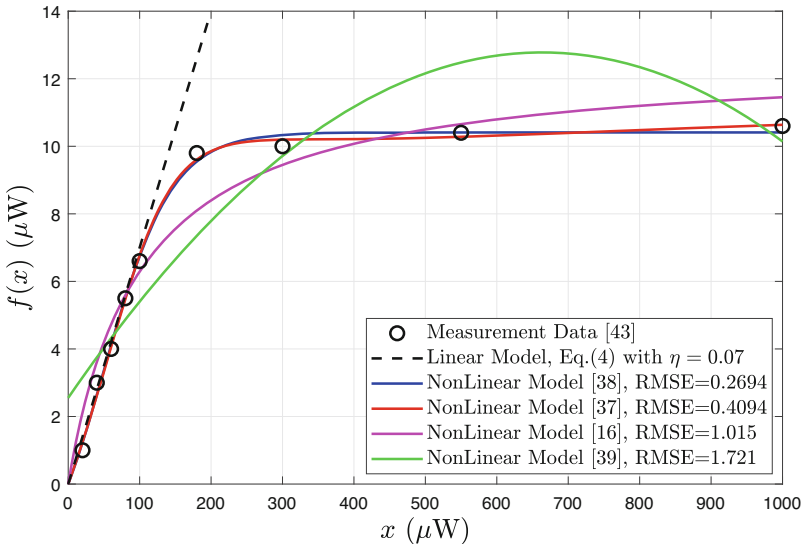


Fig. 8.8 Comparison of measurement [43] and the existing linear and nonlinear EH models

Table 8.4 System parameters for setup in Fig. 8.6

Parameter	Value	
k	20	
m	3	
δ	1	
d	0.5 bps/Hz	
λ	0.1 mssg/block	
σ^2	-70 dBm	[4]
φ	10^{-5}	
p_T	45 dBm	
ψ	-110 dB	[7]

As shown in (8.26) and (8.32), a small δ is convenient in the sense that it increases the chances of successful individual transmissions but at the same time is prejudicial by increasing the chances of concurrent transmissions. Therefore, selecting an appropriate δ is crucial for optimizing the system reliability performance. Figure 8.9 shows how the selection of δ impacts on the system reliability for different number of UEs, $k \in \{10, 100\}$, and using both, linear and nonlinear, EH models. First to notice is that there is a significant gap in the performance when using the linear vs the nonlinear EH model, thus, reinforcing the idea that the linear EH model, although suitable for analytical tractability most of the time, is idealistic and should be used with caution. For the chosen system parameter values, the FD scheme overcomes its HD counterparts using $\tau \in \{1/7, 1/4, 1/2\}$, and in all the cases as k increases, more slots are required for an efficient communication. The results shown in this figure raise an important disadvantage of the HD scheme, and it is that besides optimizing δ , the optimization over τ is also required, therefore, the HD design is even more complicated and its performance may not even reach the one achieved by the FD scheme.

Figure 8.10 shows the performance of FD and HD operating with the optimum τ as a function of the SIC parameter for $\delta \in \{1, 4\}$ and $d \in \{0.5, 1\}$ bps/Hz. Since the HD configuration does not depend on this parameter, its performance appears as a straight line. Notice that the gap in performance of HD and FD setups can be substantial when SI is efficiently eliminated, while FD is no longer suitable when SIC performance is poor, e.g., $\psi \geq -106$ dB for $\delta = 4$ and $d = 1$ bps/Hz. Even more interesting are the results shown in Fig. 8.11 where the performance appears as a function of the message arrival rate for different Line-of-Sight conditions, $m \in \{1, 4, 10\}$. As λ increases, the FD scheme becomes more suitable than HD with optimum τ as shown in Fig. 8.11a. For very small λ , HD becomes more suitable for the chosen parameter values, but notice that (1) there is still the problem of finding the optimum τ and (2) when operating with relatively large m , e.g., $m \geq 4$, the gain from using HD with optimum τ is no longer significant. Figure 8.11b shows that as λ increases, the optimum time required for WET in the HD setup decreases, and more time for information transmission is required in order to resolve the concurrent transmissions. Notice that the number of Monte Carlo samples used

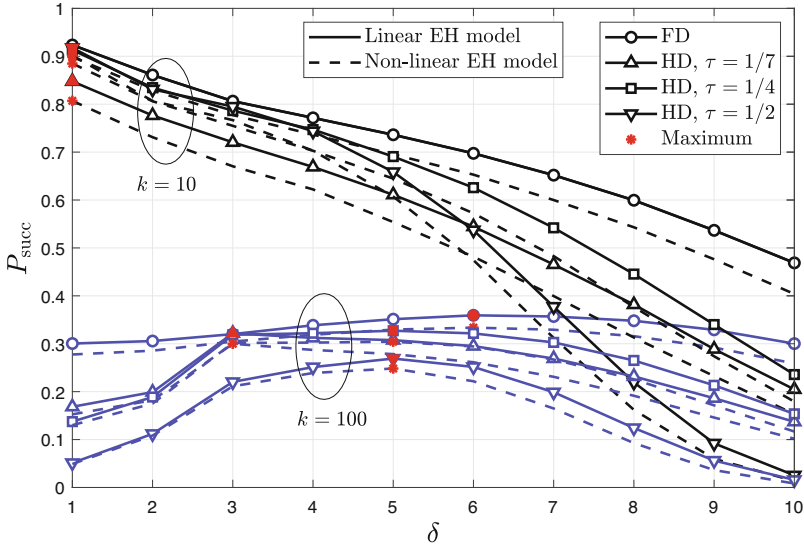


Fig. 8.9 Overall system reliability as a function of the number of transmit slots for $k \in \{10, 100\}$ and using both, linear and nonlinear, EH models. For the HD scheme we evaluated setups with $\tau = \{1/7, 1/4, 1/2\}$

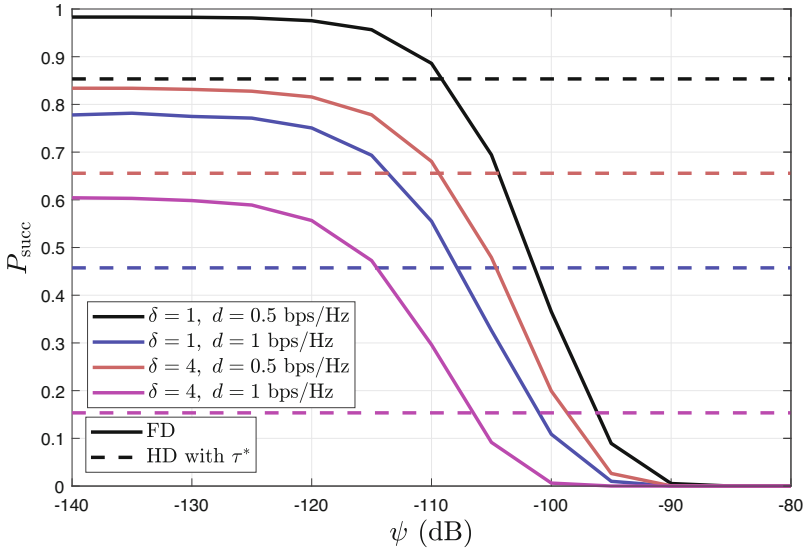


Fig. 8.10 Overall system reliability as a function of SIC parameter for $\delta \in \{1, 4\}$, $d \in \{0.5, 1\}$ bps/Hz and using nonlinear EH model. The HD performance is evaluated with the optimum τ

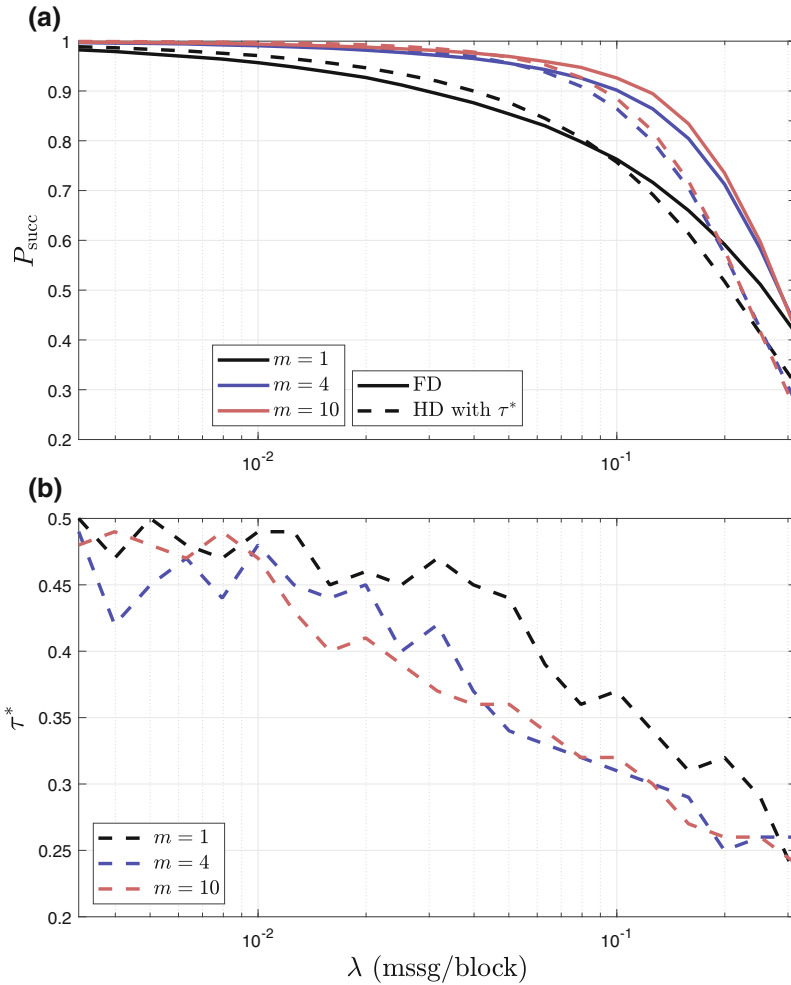


Fig. 8.11 Performance as a function of the message arrival rate for $m \in \{1, 4, 10\}$ and using nonlinear EH model. **(a)** Overall system reliability for FD and HD with the optimum τ (top) and **(b)** Optimum τ for HD scheme (bottom)

was insufficient for reaching smooth curves, but increasing such number crashes with the software and hardware limitations. Even so, the tendency can be easily appreciated, and the irregularities do not impact on the P_{succ} performance as its curves are already smooth as shown in Fig. 8.11a.

8.4 Conclusions and Outlook

In this chapter, we presented an overview of the main characteristics of the wireless-powered communication networks and the main approaches for modeling the EH conversion process. We have discussed the main FD architectures investigated in the literature, namely (1) FD bidirectional communications, (2) FD relay communications, and (3) FD hybrid AP, along with their particularities. Additionally, we have provided and analyzed two example setups related with architectures (1) and (3), while demonstrating the suitable regions for FD operation in each case. We first considered a small cell BS serving one DL and one UL users, and we demonstrated the gains in EE when the BS operates with FD for SEg recycling, especially for relatively small data rates and large transmit power in the UL and/or large transmit rate in the DL. In the second example we have considered a BS serving multiple IoT devices with a Poisson sporadic traffic pattern. For this case, we have shown that the linear EH model is optimistic and a more realistic model should be used for getting practical results. Additionally, we have compared the FD and HD schemes, and shown that the FD design is not only simpler but it also can offer significant performance gains in terms of system reliability when the SIC hardware performs not too bad.

Many possible research directions for the design and deployment of FD wireless-powered systems can be still identified. For instance: (1) Efficient MIMO implementations. MIMO techniques can be used for both, spatial-domain SIC and to harvest more energy. However, optimal solutions in FD wireless-powered systems are complex and require significant power consumption for computation purpose, even more if nonlinear EH models are used; hence, it is necessary looking at low-complexity MIMO schemes suitable for efficient FD MIMO designs. Additionally, exploiting the benefits of both, massive MIMO and FD operation in the context of wireless-powered systems, seems as an interesting direction to pursue. (2) Practical and energy-efficient FD transceiver design. Research on SI mitigation techniques with low-power consumption is essential since circuitry required in the cancellation step could drain harvested energy significantly. The nonlinear behavior of the EH circuit components needs to be taken into account for an efficient design. (3) Medium access control (MAC) layer performance. Research work on MAC layer issues is on infancy since majority of research has focused on physical-layer aspects, thus, energy-efficient FD MAC algorithms are still required. (4) Interference exploitation. In wireless-powered networks, interference may not be a completely detrimental factor, since it can be also exploited as an extra source of energy. Investigating how much interference can be exploited to improve the performance of FD wireless-powered systems is of paramount importance. Therefore, transmission schemes, scheduling, and interference cancellation algorithms that optimize the system performance taking into account these trade-offs are required.

Acknowledgements This research has been financially supported by Academy of Finland, 6Genesis Flagship (Grant no318927), and EE-IoT (no319008).

References

1. S. Priya and D. J. Inman, *Energy harvesting technologies*. Springer, 2009, vol. 21.
2. N. Shinohara, *Wireless power transfer via radiowaves*. John Wiley & Sons, 2014.
3. R. Zhang and C. K. Ho, "MIMO broadcasting for simultaneous wireless information and power transfer," *IEEE Transactions on Wireless Communications*, vol. 12, no. 5, pp. 1989–2001, May 2013.
4. Z. Hu, C. Yuan, F. Zhu, and F. Gao, "Weighted sum transmit power minimization for full-duplex system with SWIPT and self-energy recycling," *IEEE Access*, vol. 4, pp. 4874–4881, 2016.
5. A. A. Okandjeji, M. R. A. Khandaker, and K. Wong, "Wireless information and power transfer in full-duplex communication systems," in *IEEE International Conference on Communications (ICC)*, May 2016, pp. 1–6.
6. B. K. Chalise, H. A. Suraweera, G. Zheng, and G. K. Karagiannidis, "Beamforming optimization for full-duplex wireless-powered MIMO systems," *IEEE Transactions on Communications*, vol. 65, no. 9, pp. 3750–3764, Sep. 2017.
7. A. Yadav, O. A. Dobre, and H. V. Poor, "Is self-interference in full-duplex communications a foe or a friend?" *IEEE Signal Processing Letters*, vol. 25, no. 7, pp. 951–955, July 2018.
8. C. Zhong, H. A. Suraweera, G. Zheng, I. Krikidis, and Z. Zhang, "Wireless information and power transfer with full duplex relaying," *IEEE Transactions on Communications*, vol. 62, no. 10, pp. 3447–3461, Oct 2014.
9. T. N. Nguyen, D.-T. Do, P. T. Tran, and M. Vozňák, "Time switching for wireless communications with full-duplex relaying in imperfect CSI condition," 2016.
10. H. Liu, K. J. Kim, K. S. Kwak, and H. V. Poor, "Power splitting-based SWIPT with decode-and-forward full-duplex relaying," *IEEE Transactions on Wireless Communications*, vol. 15, no. 11, pp. 7561–7577, Nov 2016.
11. M. Mohammadi, H. A. Suraweera, G. Zheng, C. Zhong, and I. Krikidis, "Full-duplex MIMO relaying powered by wireless energy transfer," in *IEEE International Workshop on Signal Processing Advances in Wireless Communications (SPAWC)*, June 2015, pp. 296–300.
12. Y. Zeng and R. Zhang, "Full-duplex wireless-powered relay with self-energy recycling," *IEEE Wireless Commun. Letters*, vol. 4, no. 2, pp. 201–204, 2015.
13. M. Mohammadi, B. K. Chalise, H. A. Suraweera, C. Zhong, G. Zheng, and I. Krikidis, "Throughput analysis and optimization of wireless-powered multiple antenna full-duplex relay systems," *IEEE Transactions on Communications*, vol. 64, no. 4, pp. 1769–1785, April 2016.
14. D. Hwang, K. C. Hwang, D. I. Kim, and T. Lee, "Self-energy recycling for RF powered multi-antenna relay channels," *IEEE Transactions on Wireless Communications*, vol. 16, no. 2, pp. 812–824, Feb 2017.
15. H. Kim, J. Kang, S. Jeong, K. E. Lee, and J. Kang, "Secure beamforming and self-energy recycling with full-duplex wireless-powered relay," in *IEEE Annual Consumer Communications Networking Conference (CCNC)*, Jan 2016, pp. 662–667.
16. G. Chen, P. Xiao, J. R. Kelly, B. Li, and R. Tafazolli, "Full-duplex wireless-powered relay in two way cooperative networks," *IEEE Access*, vol. 5, pp. 1548–1558, 2017.
17. M. Gao, H. H. Chen, Y. Li, M. Shirvanimoghaddam, and J. Shi, "Full-duplex wireless-powered communication with antenna pair selection," in *IEEE Wireless Communications and Networking Conference (WCNC)*, March 2015, pp. 693–698.
18. M. A. Abd-Elmagid, A. Biazon, T. ElBatt, K. G. Seddik, and M. Zorzi, "On optimal policies in full-duplex wireless powered communication networks," in *2016 14th International Symposium on Modeling and Optimization in Mobile, Ad Hoc, and Wireless Networks (WiOpt)*, May 2016, pp. 1–7.
19. X. Kang, C. K. Ho, and S. Sun, "Full-duplex wireless-powered communication network with energy causality," *IEEE Transactions on Wireless Communications*, vol. 14, no. 10, pp. 5539–5551, Oct 2015.

20. R. Aslani and M. Rasti, "Distributed power control schemes for in-band full-duplex energy harvesting wireless networks," *IEEE Transactions on Wireless Communications*, vol. 16, no. 8, pp. 5233–5243, Aug 2017.
21. H. Kim, H. Lee, M. Ahn, H. Kong, and I. Lee, "Joint subcarrier and power allocation methods in full duplex wireless powered communication networks for OFDM systems," *IEEE Transactions on Wireless Communications*, vol. 15, no. 7, pp. 4745–4753, July 2016.
22. H. Ju and R. Zhang, "Optimal resource allocation in full-duplex wireless-powered communication network," *IEEE Transactions on Communications*, vol. 62, no. 10, pp. 3528–3540, Oct 2014.
23. H. Ju, K. Chang, and M. Lee, "In-band full-duplex wireless powered communication networks," in *International Conference on Advanced Communication Technology (ICACT)*, July 2015, pp. 23–27.
24. S. Leng, D. W. K. Ng, N. Zlatanov, and R. Schober, "Multi-objective resource allocation in full-duplex SWIPT systems," in *IEEE International Conference on Communications (ICC)*, May 2016, pp. 1–7.
25. V. Nguyen, T. Q. Duong, H. D. Tuan, O. Shin, and H. V. Poor, "Spectral and energy efficiencies in full-duplex wireless information and power transfer," *IEEE Transactions on Communications*, vol. 65, no. 5, pp. 2220–2233, May 2017.
26. M. Maso, C. Liu, C. Lee, T. Q. S. Quek, and L. S. Cardoso, "Energy-recycling full-duplex radios for next-generation networks," *IEEE Journal on Selected Areas in Communications*, vol. 33, no. 12, pp. 2948–2962, Dec 2015.
27. Z. Wen, X. Liu, N. C. Beaulieu, R. Wang, and S. Wang, "Joint source and relay beamforming design for full-duplex MIMO AF relay SWIPT systems," *IEEE Communications Letters*, vol. 20, no. 2, pp. 320–323, Feb 2016.
28. Y. L. Che, J. Xu, L. Duan, and R. Zhang, "Multiantenna wireless powered communication with cochannel energy and information transfer," *IEEE Communications letters*, vol. 19, no. 12, pp. 2266–2269, 2015.
29. Y. Bi and H. Chen, "Accumulate and jam: Towards secure communication via a wireless-powered full-duplex jammer," *IEEE Journal of Selected Topics in Signal Processing*, vol. 10, no. 8, pp. 1538–1550, Dec 2016.
30. A. A. Okandjji, M. R. A. Khandaker, K. Wong, and Z. Zheng, "Joint transmit power and relay two-way beamforming optimization for energy-harvesting full-duplex communications," in *IEEE GLOBECOM Workshops (GC Wkshps)*, Dec 2016, pp. 1–6.
31. H. Kim, J. Kang, S. Jeong, K. E. Lee, and J. Kang, "Secure beamforming and self-energy recycling with full-duplex wireless-powered relay," in *IEEE Annual Consumer Communications Networking Conference (CCNC)*, Jan 2016, pp. 662–667.
32. PowerCast. [Online]. Available: www.powercastco.com
33. C. System. [Online]. Available: <http://www.ossia.com/cota/>
34. L. R. Varshney, "Transporting information and energy simultaneously," in *2008 IEEE International Symposium on Information Theory*, July 2008, pp. 1612–1616.
35. X. Lu, P. Wang, D. Niyato, D. I. Kim, and Z. Han, "Wireless networks with RF energy harvesting: A contemporary survey," *IEEE Communications Surveys Tutorials*, vol. 17, no. 2, pp. 757–789, Secondquarter 2015.
36. X. Zhou, R. Zhang, and C. K. Ho, "Wireless information and power transfer: Architecture design and rate-energy tradeoff," *IEEE Transactions on Communications*, vol. 61, no. 11, pp. 4754–4767, November 2013.
37. Y. Chen, K. T. Sabnis, and R. A. Abd-Alhameed, "New formula for conversion efficiency of RF EH and its wireless applications," *IEEE Transactions on Vehicular Technology*, vol. 65, no. 11, pp. 9410–9414, Nov 2016.
38. E. Boshkovska, D. W. K. Ng, N. Zlatanov, and R. Schober, "Practical non-linear energy harvesting model and resource allocation for SWIPT systems," *IEEE Communications Letters*, vol. 19, no. 12, pp. 2082–2085, Dec 2015.
39. X. Xu, A. Özçelikale, T. McKelvey, and M. Viberg, "Simultaneous information and power transfer under a non-linear RF energy harvesting model," in *IEEE International Conference on Communications (ICC)*, May 2017, pp. 179–184.

40. O. L. A. López, H. Alves, R. D. Souza, and S. Montejo-Sánchez, “Statistical analysis of multiple antenna strategies for wireless energy transfer,” *arXiv preprint arXiv:1811.10308*, 2018, <https://ieeexplore.ieee.org/abstract/document/8760520>.
41. H. G. Schantz, “Near field propagation law & A novel fundamental limit to antenna gain versus size,” in *IEEE Antennas and Propagation Society International Symposium*, vol. 3A, July 2005, pp. 237–240 vol. 3A.
42. F. Boccardi, R. W. Heath, A. Lozano, T. L. Marzetta, and P. Popovski, “Five disruptive technology directions for 5G,” *IEEE Communications Magazine*, vol. 52, no. 2, pp. 74–80, February 2014.
43. T. Le, K. Mayaram, and T. Fiez, “Efficient far-field radio frequency energy harvesting for passively powered sensor networks,” *IEEE Journal of Solid-State Circuits*, vol. 43, no. 5, pp. 1287–1302, May 2008.